

# Colloidal Silicalite Coating for Improving Ionic Liquid Membrane Loading on Macroporous Ceramic Substrate for Gas Separation

Zishu Cao, Shaowei Yang, Xinhui Sun, Antonios Arvanitis and Junhang Dong\*

Department of Chemical Engineering, University of Cincinnati, Cincinnati, Ohio 45221, USA

**Abstract:** A thin layer of colloidal silicalite was coated on a macroporous alumina substrate to improve the effectiveness in loading and supporting ionic liquid (IL) membrane on macroporous ceramic substrate. The [bmim][BF<sub>4</sub>] IL and CO<sub>2</sub> gas separation were used as the model system in this research. The colloidal silicalite top layer enabled the formation of a pinhole-free IL membrane with significantly reduced load of IL as compared to the bare alumina substrate because the former had a smaller and more uniform inter-particle pore size than the latter. The supported IL membrane was extensively studied for CO<sub>2</sub> separation in conditions relevant to coal combustion flue gases. The silicalite-supported IL membrane achieved a CO<sub>2</sub>/N<sub>2</sub> permselectivity of ~24 with CO<sub>2</sub> permeance of  $\sim 1.0 \times 10^{-8}$  mol/m<sup>2</sup>·s·Pa in dry conditions at 26°C and reached a CO<sub>2</sub>/N<sub>2</sub> separation factor of ~18 with CO<sub>2</sub> permeance of  $\sim 1.56 \times 10^{-8}$  mol/m<sup>2</sup>·s·Pa for a feed mixture containing ~11% CO<sub>2</sub> and ~9% water vapor at 50°C. This supported IL membrane exhibited excellent stability under a 5-bar transmembrane pressure at 103°C and chemical resistance to H<sub>2</sub>O, SO<sub>2</sub>, and air (O<sub>2</sub>). Results of this study also indicated that, in order to fully realize the advantages of using the colloidal silicalite support for IL membranes, it is necessary to develop macroporous ceramic supports with optimized pore size distribution so that the IL film can be retained in the micron-thin silicalite layer without penetrating into the base substrate.

**Keywords:** Colloidal silicalite, ionic liquid, membrane, carbon dioxide, separation.

## 1. INTRODUCTION

Coal-firing power plants are responsible for roughly a third of the human-made CO<sub>2</sub> emission into the atmosphere and this situation is expected to continue in the foreseeable future. CO<sub>2</sub> capture and sequestration (CCS) for coal-firing plants is therefore critical to mitigation of CO<sub>2</sub> emission. For the large number of existing coal-firing power plants, success of CO<sub>2</sub> capture will depend on the availability of cost-effective technologies for CO<sub>2</sub> separation from N<sub>2</sub> and a number of coexisting gas impurities. Despite the extensive research and development efforts made in the past decades, existing CO<sub>2</sub> separation technologies, such as solvent scrubbing, pressure or temperature swing adsorption, and CO<sub>2</sub>-selective membrane permeation, are not economically viable for industrial scale CCS application unless highly value-added CO<sub>2</sub> reuse is realized to offset the cost [1-3]. In searching for more energy-efficient and environmentally friendly CO<sub>2</sub>-capture methods, ionic liquids (ILs) have recently attracted broad interests as a new type of absorbents and liquid membrane materials for CO<sub>2</sub> separations [4]. ILs are liquid state salts whose molecules typically consist of an organic cation and an inorganic or organic anion. ILs are considered green solvents because of their nontoxic nature, extremely low vapor pressures, and thermal stability up to a few

hundred degrees Celsius. Many ILs were found to dissolve CO<sub>2</sub> with high selectivity over other gases involved in coal-firing flue gases except for SO<sub>2</sub> which may have higher solubility than CO<sub>2</sub> in amine type ionic liquids [4, 5]. The dissolved CO<sub>2</sub> molecule locates between the cation and anion of the IL and the weak CO<sub>2</sub>-IL interaction, primarily van de Waals force, allows for CO<sub>2</sub> desorption without significant heat consumption [6]. However, industrial applications of the IL as solvents in scrubbing processes have been so far discouraged by the prohibitive cost for large volumes of expensive IL needed and low mass transfer rates caused by their high viscosity [1, 6]. A potentially more effective way of utilizing ILs for CO<sub>2</sub> separation is to construct supported IL membranes, which could offer a number of advantages including minimal amount of IL usage, continuous operation mode, stability in porous support, and better energy efficiency and readiness of the membrane unit operation for retrofitting existing plants.

Supported IL membranes are typically formed by loading ILs in porous substrates of polymeric or ceramic materials using liquid impregnation or infiltration techniques. There have been reports on the use of porous hollow fibers as IL supports to achieve large membrane packing densities that are critical to large scale applications [3, 7-9]. The number of publications on IL solvent and membrane development for CO<sub>2</sub> separations has been fast growing for the past few years but the research efforts were largely focused on measuring thermodynamic and transport properties, studying CO<sub>2</sub> selectivity and permeance for pure gases

\*Address correspondence to this author at the Department of Chemical Engineering, University of Cincinnati, Cincinnati, Ohio 45221, USA;  
Tel: +1 (513) 556-3992; Fax: +1 (513) 556-3473;  
E-mail: Junhang.dong@uc.edu

and simple binary mixtures, and synthesizing new or modifying existing ILs for enhanced separation performances. Studies on the influence of substrate on IL membrane formation and gas transport properties of the supported IL membrane in conditions relevant to practical CO<sub>2</sub> separation from coal combustion flue gas have been quite limited.

Coal-combustion flue gases are typically at atmospheric pressure and 50 – 100°C, containing 70–75% N<sub>2</sub>, 10–15% CO<sub>2</sub>, 5–10% H<sub>2</sub>O, and 3–4% O<sub>2</sub> with ppm-level CO (~20 ppm), SO<sub>x</sub> (<500 ppm) and NO<sub>x</sub> (<800 ppm) [6]. The relatively low CO<sub>2</sub> partial pressure necessitates either compressing of the flue gas in feed side or vacuuming the permeate side to drive the CO<sub>2</sub> transport through the membrane. Also, with the low CO<sub>2</sub> concentration in the flue gases, multi-stage membrane operation is usually needed for achieving the targeted goal of >90% recovery and >95% purity in combustion flue gas CO<sub>2</sub> capture because of the limited CO<sub>2</sub>/N<sub>2</sub> selectivity ( $\alpha_{CO_2/N_2}$ ) and permeance ( $P_{m,CO_2}$ ) of current CO<sub>2</sub>-separation membranes [3]. Furthermore, many imidazolium salts such as those containing [PF<sub>6</sub>] anion were found to decompose in the presence of O<sub>2</sub> even at low temperatures [10]. IL membranes need to be experimentally evaluated in more practically relevant conditions such the presence of air and water vapor at various compositions, pressures, and temperatures to understand the performance and stability. Also, since the IL membrane is retained in the porosity of the substrate, the material properties and pore structure of the support can play an important role in determining the overall membrane performance, identification and improvement of the substrate is thus necessary.

Here we reported the fabrication of 1-*n*-butyl-3-methylimidazolium tetrafluoroborate ([bmim][BF<sub>4</sub>], C<sub>8</sub>H<sub>15</sub>F<sub>4</sub>N<sub>2</sub>B) IL membrane supported on a colloidal silicalite coated macroporous alumina disc and experimental investigations on its CO<sub>2</sub> separation performance under various conditions relevant to CO<sub>2</sub> capture from coal-combustion flue gas. The hypothesis is that, because the liquid film is held inside the porous substrate by capillary action, the colloidal silicalite layer with small inter-particle pore size can improve IL membrane formation with reduced IL loading and effective IL membrane thickness. The silicalite is a pure-silica MFI-type zeolite containing channels of ~0.56-nm in diameter, which are inaccessible to the large IL molecules, with hydrophobic surface that are also known to be CO<sub>2</sub>-permselective; thus the use of colloidal silicate layer as support may also benefit the

overall CO<sub>2</sub> separation performance of the supported IL membrane. The [bmim][BF<sub>4</sub>] IL was chosen for the present research because of its high CO<sub>2</sub> sorption capacity and selectivity, good chemical stability in the presence of H<sub>2</sub>O, O<sub>2</sub>, SO<sub>x</sub>, and NO<sub>x</sub>, etc., and extensive thermodynamic and transport properties accessible in open literature [6].

## 2. EXPERIMENTAL

### 2.1. Membrane Preparation and Characterization

The colloidal silicalite layers were coated on homemade porous  $\alpha$ -alumina discs using a similar procedure as described in a previous publication [11]. The alumina disc was 2-mm thick and 25 mm in diameter, which had an average pore size of ~85 nm and porosity ( $\epsilon$ ) of 27~30%. The disc edge was sealed with dense glass coating and the active membrane area ( $A_m$ ) after excluding the sealing area was 2.54 cm<sup>2</sup>. The silicalite nanoparticles were synthesized by in situ hydrothermal crystallization of a precursor, which had a molar composition of 0.33(SiO<sub>2</sub>): 0.1(tetrapropylammonium hydroxide): 0.035(NaOH): 5.56(H<sub>2</sub>O), where tetrapropylammonium hydroxide (TPAOH) is the structure directing agent (SDA) [12]. The precursor was obtained by dissolving fumed silica (99.8%, 0.007  $\mu$ m, Aldrich) and NaOH pellets (99.998%, Aldrich) in 1 M TPAOH solution (Aldrich) at 80 °C. The precursor was hydrothermally reacted in an autoclave at 60 °C for 15 days. After crystallization, the resultant silicalite nanoparticles were washed by DI water and recovered using centrifuge.

The silicalite nanoparticles were dispersed in DI water and peptized by 1 M HNO<sub>3</sub> solution. Hydroxyl propyl cellulose (HPC, Mw = 100,000, Aldrich) was used as the drying control agent (DCA) to prevent the crack formation in the dip-coated colloidal film in the drying and calcination processes. The pH of the final silicalite colloidal suspension for film coating was in a range of 3 ~ 4 and the contents of silicalite particle and HPC were 0.4wt% and 0.2wt%, respectively. The dip-coating process used a contact time of 5 s. The dip-coated membrane was dried in an oven at 40 °C for 24 h and then calcined in air at 450 °C for 6 h to remove the SDA (TPAOH) from zeolitic pores, burn off the HPC binder, and consolidate the colloidal silicalite layer. The dip-coating, drying and calcining process was repeated once to eliminate possible pinholes in the first coating and obtain desired thickness. The colloidal suspension used for the second coating contained 0.2wt% silicalite particle while other compositions kept unchanged. The

remaining of the silicalite suspension used in the first dip-coating process was dried at 40 °C and fired together with the dip-coated discs to obtain an unsupported colloidal silicalite film. This unsupported film and the porous alumina substrate was tested by Brunauer–Emmett–Teller (BET) porosimetry (ASAP2020, Micromeritics) to characterize the pore size distribution (PSD).

The [bmim][BF<sub>4</sub>] was loaded into the silicalite-coated side of the disc by manually brushing IL on the colloidal silicalite membrane surface and removing the excessive IL using a dry brush followed by gently wiping with powder-less cleaning tissue. The amount of the IL loaded into to the substrate was determined by weighing the disc before and after coating the IL. The same coating process was also performed to load IL into the bare alumina substrate without the silicalite top layer.

To confirm the type of gas absorption in the IL membrane, the [bmim][BF<sub>4</sub>] IL was examined by Fourier transform infrared spectroscopy (FTIR; Shimadzu IRPrestige-21 FTIR spectrophotometer equipped with an attenuated total reflectance (ATR) unit) after absorbing different gases, including N<sub>2</sub>, CO<sub>2</sub>, SO<sub>2</sub>, and H<sub>2</sub>O. The IR spectra were collected in a wavenumber range of 400–4000 cm<sup>-1</sup> at a resolution of 4 cm<sup>-1</sup>. During the experiments, the pure [bmim][BF<sub>4</sub>] was degassed by purging/bubbling with He (20 ml/min) at 120 °C for 8 h followed by vacuuming for an hour before being cooled down to absorb each gas. The gas absorption was accomplished by bubbling the testing gas stream (10 ml/min) through 1 ml of the IL in a small test tube for ~12 h. The gas-absorbed IL was sealed in the tube for immediate FTIR examination. After the FTIR measurement, the IL was degassed and re-examined by FTIR to test the reversibility of the gas sorption.

## 2.2. Gas Permeation Measurements

The supported IL membrane was tested for single gas permeation and CO<sub>2</sub> separation from a variety of mixtures using an apparatus shown in Figure 1, which was modified from our previously reported membrane reactor system [13]. The supported IL was mounted in a stainless steel cell by O-ring seals and the side of the colloidal silicalite layer loaded with IL was placed facing upward. The feed flow rate was regulated by a mass flow controller. When high pressure was used on the feed side, the feed flow rate was monitored by a bubble flow meter installed after the backpressure controller. The exiting streams from both the feed (retentate) and permeate sides were analyzed by an online gas

chromatograph (GC). The permeate side of the membrane was either swept by a helium flow or vacuumed to create transmembrane partial pressure difference, i.e.,  $\Delta P_i = \Delta P_{i,f} - \Delta P_{i,p}$ , where  $P_{i,f}$  and  $P_{i,p}$  are the partial pressures of gas component  $i$  in the feed and permeate sides, respectively. When a sweeping gas was used, the composition and flux of the permeate stream was measured by the online GC. The entire membrane cell was housed in an oven for temperature control and preheating coils were used to ensure that the feed and sweeping gases reached setting temperature before contacting the membrane. The permeance of gas  $i$  ( $P_{m,i}$ ), CO<sub>2</sub> permeaselectivity against gas  $j$  ( $\alpha_{CO_2/j}^o$ ), and CO<sub>2</sub> separation factor over gas  $j$  ( $\alpha_{CO_2/j}$ ) are defined as following:

$$P_{m,i} = \frac{Q}{A_m \cdot t \cdot \Delta P_i} \quad (1)$$

$$\alpha_{CO_2/j}^o = P_{m,CO_2}^o / P_{m,j}^o \quad (j \neq CO_2) \quad (2)$$

$$\alpha_{CO_2/j} = \frac{(y_{CO_2} / y_j)}{(x_{CO_2} / x_j)} \quad (j \neq CO_2) \quad (3)$$

where  $Q$  (mol) is the amount of component  $i$  permeated through the membrane over a time period of  $t$  (s);  $P_{m,CO_2}^o$  and  $P_{m,j}^o$  are single gas permeance of CO<sub>2</sub> and gas  $j$ , respectively; and  $x$  and  $y$  are molar compositions of the feed and permeate gas mixtures, respectively.

### Single Gas Permeation as a Function of Temperature

Single gas permeation was measured for N<sub>2</sub>, O<sub>2</sub>, CO<sub>2</sub> at 25, 40, 60, 80, 100 and 120 °C, respectively. The entering feed flow rate was 20 cm<sup>3</sup> (STP)/min and the permeate side sweeping gas (Helium) flow rate was 10 cm<sup>3</sup> (STP)/min. Before the permeation test for each gas, the membrane was degassed by purging both sides with pure helium at 120 °C for overnight [14]. The permeation measurement was first performed from low temperature to high temperature and then repeated from high temperature to low temperature to examine the reversibility and reproducibility of the membrane permeation behavior.

### CO<sub>2</sub> Separation from Binary Mixtures

CO<sub>2</sub> separation was performed for CO<sub>2</sub>/N<sub>2</sub> binary mixtures and CO<sub>2</sub>/Air mixtures. For both types of mixtures, the feed flow rate was 20 cm<sup>3</sup> (STP)/min and the Helium sweeping flow rate was 10 cm<sup>3</sup> (STP)/min. For the separation of N<sub>2</sub>/CO<sub>2</sub> mixture, both sides of the membrane were at ambient pressure and the CO<sub>2</sub> mole

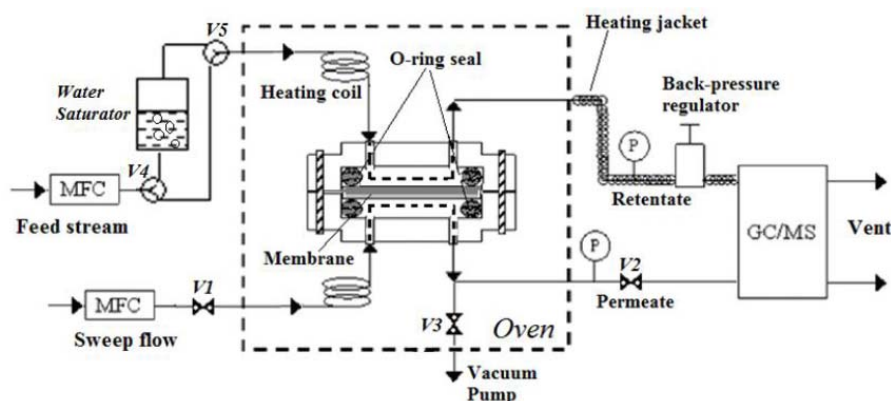


**Figure 1:** Schematic diagram of the membrane gas permeation measurement system.

fraction in the feed ( $x_{CO_2}$ ) was varied at 0.05, 0.10, 0.15, 0.25, 0.50 and 0.75, respectively. The separation experiments were conducted at 26 and 53°C, respectively. The CO<sub>2</sub>/air mixture contained a fixed composition of 20mol% CO<sub>2</sub> and 80mol% dry air. Separation of the CO<sub>2</sub>/air mixture was performed at temperature of 25, 40, 60, 80 and 100°C, respectively. The gas separation experiments were first conducted as temperature increased and then repeated as temperature decreased to observe the reversibility and reproducibility of the membrane performance. At each temperature, the separation of CO<sub>2</sub>/air mixture was conducted at various feed side pressures ranging from 1 bar to 6 bar with ambient pressure on the permeate side.

### **CO<sub>2</sub> Separation from Mixtures Containing Impurities**

The effects of water vapor and trace SO<sub>2</sub> in the feed on the membrane separation of CO<sub>2</sub> were tested. The CO<sub>2</sub>/N<sub>2</sub> mixture was bubbled through the water vapor saturator at a flow rate of 8 cm<sup>3</sup> (STP)/min of dry gas before entering the membrane cell. The permeate side of the membrane was swept by Helium at a flow rate of 5 cm<sup>3</sup> (STP)/min. The separation of the humid CO<sub>2</sub>/N<sub>2</sub> mixtures was performed at 50 °C for mixtures with various CO<sub>2</sub> mole fractions of 0.1, 0.3, 0.5 and 0.7, respectively. This temperature was well above that of the water vapor saturator to prevent water condensation in the porous membrane substrate. The temperature of the water vapor saturator was varied at 35 °C and 44 °C to obtain different water vapor partial pressures ( $P_{H_2O}$ ) of 5.6 kPa and 9 kPa, respectively. The effect of SO<sub>2</sub> was tested using a commercially obtained mixture containing 500 ppmv SO<sub>2</sub>, 20% CO<sub>2</sub>, and balance Air (prepared and certified by Matheson Tri-Gas, OH). This multicomponent gas was fed at a flow rate of 20 cm<sup>3</sup> (STP)/min when the permeate side

was swept by Helium at flow rate of 10 cm<sup>3</sup> (STP)/min. The gas separation experiments were performed at 25, 40, 60, 80 and 100 °C, respectively, along both ways as temperature increasing and then decreasing. The gas separation was also performed by varying the feed pressure from 1 to 6 bars at each temperature while the permeate side was kept at ambient pressure.

### **CO<sub>2</sub> Separation with Vacuum Pressure on Permeate Side**

In practical applications, the driving force  $\Delta P_i$  can be maintained by pressurizing the feed and/or using vacuum pressure on the permeate side but not by an inert gas sweep, which may require additional separation afterward. Using vacuum pressure on the permeate side may be advantageous over upstream pressurization in CO<sub>2</sub> separation from flue gases because the former requires much less volumetric work as the mass of permeate is far less than the mass of feed. The permeate side was maintained at a nearly constant pressure of 0.5 kPa by a vacuum pump in the experiment. The feed stream was an equimolar CO<sub>2</sub>/N<sub>2</sub> mixture at a total flow rate of 6 cm<sup>3</sup> (STP)/min. The membrane separation was tested at 25, 40, 60, 80 and 100 °C, respectively, both during temperature increasing and then decreasing processes. The flux and composition of the permeate gas were obtained based on the flow rates of the feed inlet and outlet monitored by a bubble flow meter and their compositions analyzed by the online GC. The permeate gas flow rate and composition were then obtained by mass balance calculations.

## **3. RESULTS AND DISCUSSION**

### **3.1. Supported IL Membranes**

The silicalite particles obtained by in situ hydrothermal crystallization were nearly spherical with

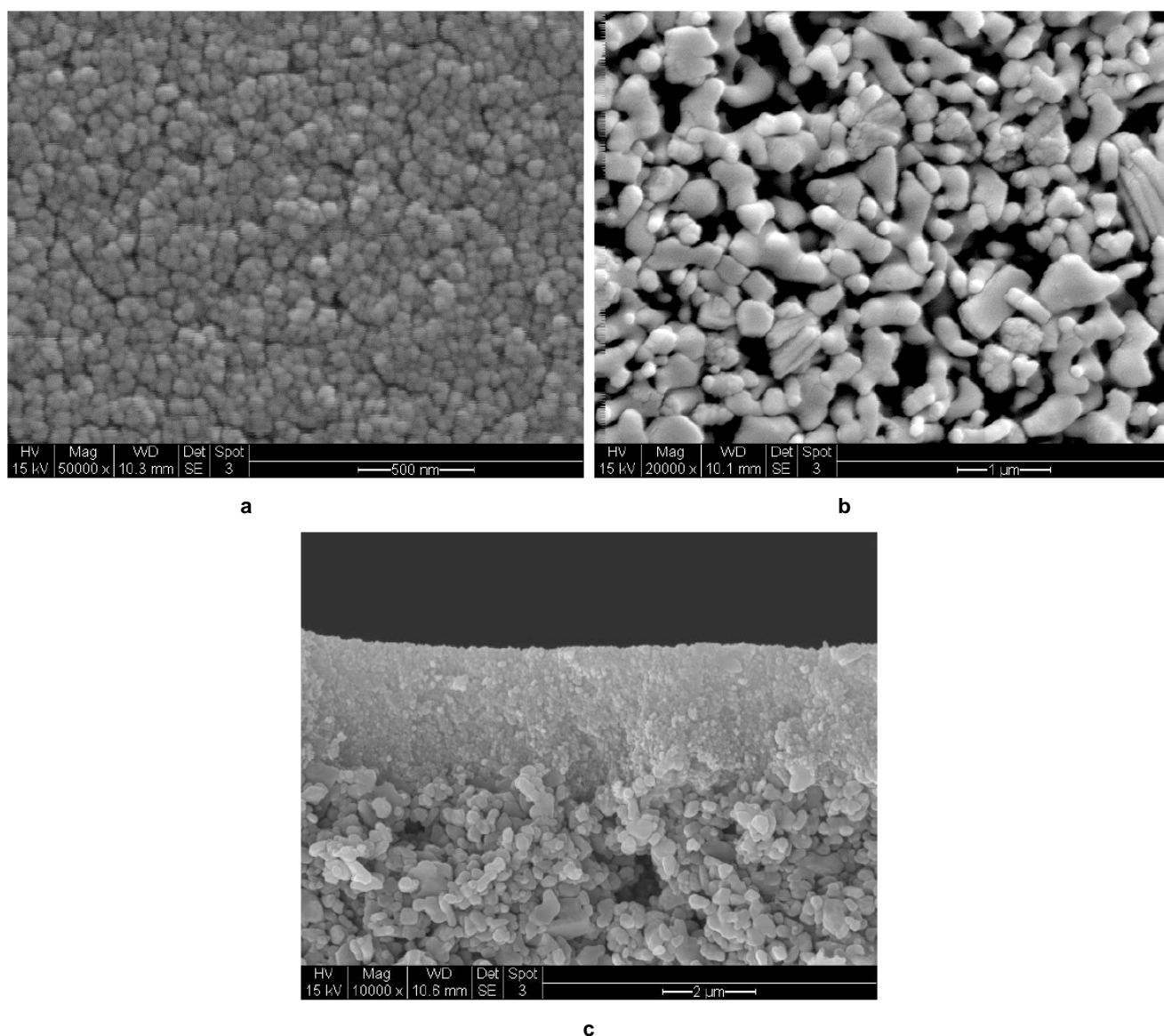


**Figure 2:** SEM images of a colloidal silicalite layer on porous alumina disc: (a) – surface of silicalite layer; (b) – surface of alumina substrate, and (c) – cross-section of silicalite-coated substrate.

an average diameter of  $\sim 80$  nm. Figure 2 shows the scanning electron microscopy (SEM) images of the colloidal silicalite film coated on the porous alumina disc by the two-step dip-coating process. The colloidal silicalite layer was  $\sim 3$   $\mu\text{m}$  in thickness and no pinholes and cracks were observed by extensive SEM scanning over a sample area of  $3000 \mu\text{m} \times 3000 \mu\text{m}$ . Figure 3 shows the PSD of the silicalite film and alumina support obtained by BET measurements using  $\text{N}_2$  adsorption and desorption at 77 K. The unsupported silicalite film had an inter-particle pore porosity ( $\epsilon_z$ ) of  $\sim 20\%$ , PSD in the range of 10 to 40 nm with an average pore size ( $d_{p,z}$ ) of  $\sim 25$  nm; the alumina substrate had a pore porosity ( $\epsilon_s$ ) of  $\sim 28\%$  and a broad PSD ranging from 10 to 130 nm with an apparent average pore size ( $d_{p,s}$ ) of  $\sim 85$  nm. A small number of large pores or voids with

size of  $0.5 - 1.0 \mu\text{m}$  were found in the SEM picture of the substrate cross section in Figure 2 (c).

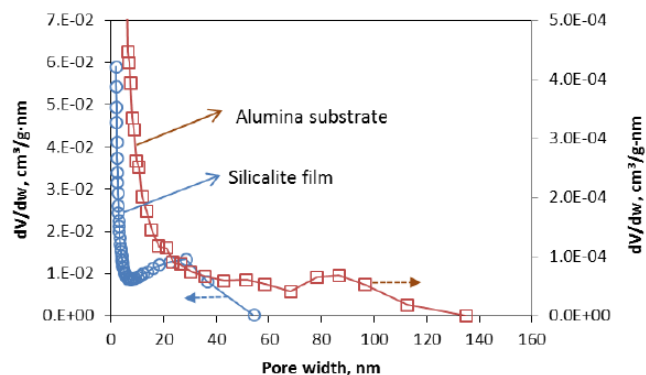


**Figure 3:** Pore size distributions of the unsupported colloidal silicalite layer and the alumina substrate.

**Table 1: Single Gas Permeation Results for the Colloidal Silicalite-Coated Alumina Disc and the Bare Alumina Substrate with Different IL Loadings (at 25 °C)**

Substrate for IL	IL load, mg/cm <sup>2</sup>	IL $\delta^*$ , mm	$P_{m,N_2} \cdot 10^{-10}$ , mol/m <sup>2</sup> ·s·Pa	$P_{m,CO_2} \cdot 10^{-10}$ , mol/m <sup>2</sup> ·s·Pa	$\alpha_{CO_2/N_2}^o$
Silicalite-coated alumina	0	None	~3,000	~2,700	0.9
Silicalite-coated alumina	13±1	0.317	39.3	112	2.85
Silicalite-coated alumina	20±1	0.499	3.52	62.7	17.8
Bare alumina disc	0	None	~11,400	~10,900	0.96
Bare alumina disc	19±1	0.461	876	877	1.0
Bare alumina disc	37±1	0.910	385	431	1.1
Bare alumina (Fully soaked)	83±1	2.06	0.987	0.596	0.6

\*Nominal thickness of IL film in substrate (i.e. depth of the IL fill in substrate) estimated by  $\delta = m_{IL} / (\rho_{IL} \cdot A_m \cdot \varepsilon)$  where  $m_{IL}$  is the mass of loaded IL;  $\rho_{IL}$  is the IL density;  $A_m$  is the total membrane area, and  $\varepsilon$  is the porosity.

The results of N<sub>2</sub> and CO<sub>2</sub> single gas permeation tests for the membranes with various IL loading levels are summarized in Table 1.

Before loading IL, the silicalite-coated disc exhibited very high  $P_{m,N_2}$  and  $P_{m,CO_2}$  with an  $\alpha_{CO_2/N_2}^o$  only slightly greater than the Knudsen diffusion selectivity ( $\alpha_{CO_2/N_2,Knudsen}^o = \sqrt{M_{W_{N_2}}/M_{W_{CO_2}}} = 0.8$ , i.e. N<sub>2</sub>-selective) because the gas flux was primarily through the nanometer scale inter-particle pores with minor contribution from the preferential adsorption and diffusion of CO<sub>2</sub> through the 0.56 nm-diameter zeolitic pores [15]. A continuous and pinhole-free [bmim][BF<sub>4</sub>] IL membrane was obtained in this colloidal silicalite-coated substrate with an IL-load of 20 mg/cm<sup>2</sup>. The formation of a pinhole-free IL film at IL-load of 20 mg/cm<sup>2</sup> was evidenced by the sharply decreased N<sub>2</sub> permeance ( $P_{m,N_2}$ ) with dramatically increased  $\alpha_{CO_2/N_2}^o$  as compared to the corresponding values of the disc with no IL and with an IL load of 13 mg/cm<sup>2</sup>. The  $P_{m,N_2}$  and  $\alpha_{CO_2/N_2}^o$  changed from  $3 \times 10^{-7}$  mol/m<sup>2</sup>·s·Pa and 0.9 respectively, before loading IL, to  $3.52 \times 10^{-10}$  mol/m<sup>2</sup>·s·Pa and 17.8, respectively, after loading 20 mg-IL/cm<sup>2</sup>. In contrast, no continuous pinhole-free IL films could be formed in the bare alumina substrate with IL loads of 19 and 37 mg/cm<sup>2</sup> as indicated by the very high  $P_{m,N_2}$  of  $8.76 \times 10^{-8}$  mol/m<sup>2</sup>·s·Pa and  $3.85 \times 10^{-8}$  mol/m<sup>2</sup>·s·Pa and low  $\alpha_{CO_2/N_2}^o$  of 1.0 and 1.1 at the two levels of IL loading, respectively. Clearly, the biggest pores in the alumina disc cannot be closed until the disc is fully soaked with IL because of its broad PSD and irregular pore geometry. However, when the alumina disc was fully soaked with IL, the gas flux became extremely small ( $< 10^{-10}$  mol/m<sup>2</sup>·s·Pa) due to vary large IL film thickness; and thus, the possible very small gas leak through the seals might have caused vary large errors in gas permeation measurements.

The single gas permeation results of the supported IL membranes demonstrated that the colloidal silicalite layer enabled the formation of pinhole-free IL membrane with reduced IL load with which a continuous IL film was unable to form in the bare alumina substrate. The smaller and more uniform inter-particle pores of the silicalite layer can soak and retain the IL by stronger capillary action to prevent the IL from entering the larger pores in the alumina substrate. However, due to the partial overlap of PSD between the silicalite layer and alumina substrate, the alumina disc would obviously take most of the loaded IL before completely filling the relatively larger pores in the silicalite layer. The IL membrane formed on the silicalite-coated alumina disc by loading 20 mg-IL/cm<sup>2</sup> (Table 1) is denoted as Sil-IL20 hereafter. All gas permeation and CO<sub>2</sub> separation tests reported here were obtained on this membrane.

### 3.2. Single Gas Permeation

The membrane Sil-IL20 was tested for single gas permeation of N<sub>2</sub>, O<sub>2</sub>, and CO<sub>2</sub>, respectively, at temperatures ranging from 25 to 120 °C. Figure 4 shows the single gas permeance and CO<sub>2</sub> permselectivity over N<sub>2</sub> and O<sub>2</sub>, i.e.  $\alpha_{CO_2/N_2}^o$  and  $\alpha_{CO_2/O_2}^o$ , as a function of temperature.

The gas permeance and permselectivity obtained during temperature increasing and decreasing processes were found to be generally consistent, demonstrating that the IL membrane supported on the colloidal silicalite layer was thermally stable and the gas transport properties were reversible in the tested temperature range of 25 – 120 °C. Within this range, the permeances of all three gases increased whilst both  $\alpha_{CO_2/N_2}^o$  and  $\alpha_{CO_2/O_2}^o$  decreased monotonically with

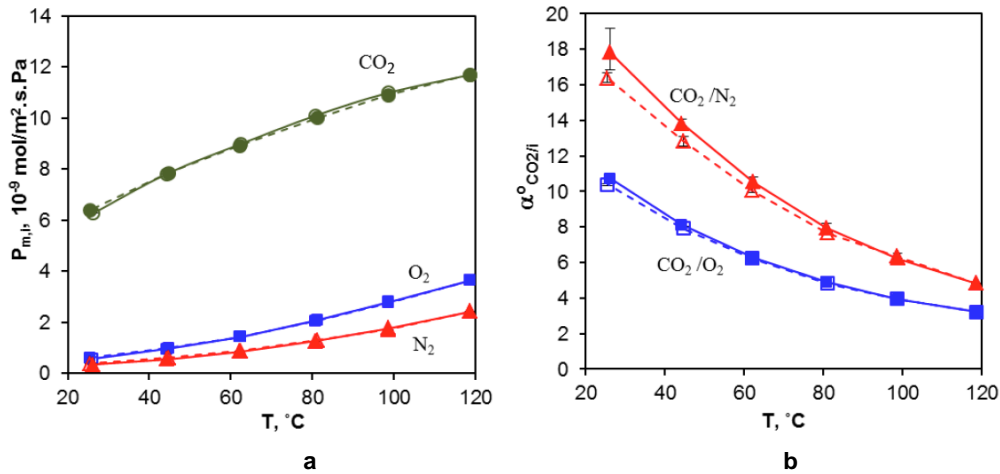


**Figure 4:** Single gas permeation through membrane Sil-IL20 as a function of temperature (closed symbols – measured when increasing temperature; open symbols – measured when decreasing temperature): (a) gas permeance and (b)  $\text{CO}_2$ -permselectivity.

increasing temperature. These temperature dependencies of  $\text{CO}_2$  permeance and permselectivity are resulted from the solution-diffusion mechanism. In general, the permeability of gas  $i$  in the membrane ( $P_{b,i}$ ) is given by  $P_{b,i} = C_i \times D_i$ , where  $C_i$  and  $D_i$  are respectively the gas solubility ( $\text{mol/m}^3 \cdot \text{Pa}$ ) and diffusivity ( $\text{m}^2/\text{s}$ ) in the membrane material. For  $\text{CO}_2$ ,  $C_i$  decreases and  $D_i$  increases in [bmim][ $\text{BF}_4$ ] IL with increasing temperature [16]. The gas permeation results in Figure 4 suggest that the effect of diffusivity enhancement overpowered the countering effect of solubility decrease on the gas permeability as temperature increasing from 25 to 120  $^{\circ}\text{C}$ . The same effects of  $C_i$  decrease and  $D_i$  increase on gas diffusion through the zeolitic pore of the silicalite are expected as temperature increases. The apparent activation energies ( $E_a$ ) of gas permeation through the Sil-IL20 membrane obtained from the Arrhenius plot of gas fluxes in Figure 5 were 6.58, 19.75, and 19.15 kJ/mol for  $\text{CO}_2$ ,  $\text{N}_2$  and  $\text{O}_2$ , respectively. The apparent activation energy of gas permeation depends on the combination of heat of absorption ( $Q_a < 0$ ) and diffusion activation energy ( $E_d > 0$ ). The smaller  $E_a$  of  $\text{CO}_2$  as compared to those of  $\text{N}_2$  and  $\text{O}_2$  may be attributed to the fact that  $\text{CO}_2$  is preferentially absorbed to give negatively larger  $Q_a$  and  $\text{CO}_2$  transport in the IL is facilitated by the ionic carriers while  $\text{N}_2$  and  $\text{O}_2$  are weakly absorbing and their transport in the IL is non-facilitated. The activation energy of  $\text{CO}_2$  permeation through the supported [bmim][ $\text{BF}_4$ ] IL membrane was very close to the diffusion activation energy in the bulk IL ( $\sim -6.0$  kJ/mol) [16]. This observation is consistent with findings in the literature where  $\text{CO}_2$  diffusivity in IL filled in nanoporous silica substrate was reported to be similar to or slightly greater than that in the bulk IL [17]. Because the apparent diffusion activation energies of  $\text{N}_2$  and  $\text{O}_2$  are much larger than that of the  $\text{CO}_2$ , increasing temperature causes greater permeability

enhancement for  $\text{N}_2$  and  $\text{O}_2$  than for  $\text{CO}_2$ , leading to decline of  $\text{CO}_2$  permselectivity.

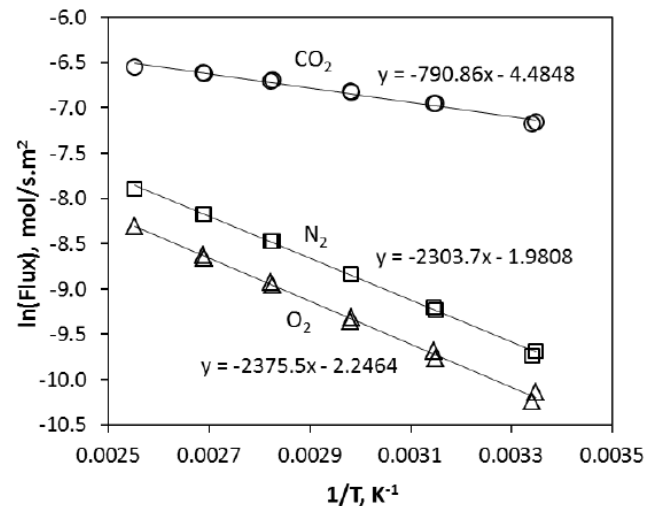


**Figure 5:** Temperature dependences of single gas flux through the SIL-IL20 membrane.

### 3.3. Separation of $\text{CO}_2/\text{N}_2$ Mixtures

The SIL-IL20 membrane was tested for separation of  $\text{N}_2/\text{CO}_2$  binary mixtures as a function of  $\text{CO}_2$  mole fraction ( $x_{\text{CO}_2}$ ) in the feed under atmospheric pressure at 26 and 53  $^{\circ}\text{C}$ , respectively. Figure 6 presents the results of individual gas permeance ( $P_{m,\text{CO}_2}$ ) and  $\text{CO}_2$  separation factor  $\alpha_{\text{CO}_2/\text{N}_2}$  as a function of  $x_{\text{CO}_2}$ . The  $\alpha_{\text{CO}_2/\text{N}_2}$  was higher and  $P_{m,\text{CO}_2}$  was lower at 26  $^{\circ}\text{C}$  than was at 53  $^{\circ}\text{C}$  that is consistent with the temperature dependencies of  $\alpha_{\text{CO}_2/\text{N}_2}$  and  $P_{m,\text{CO}_2}^{\circ}$  found in single gas permeation tests. For the feed containing 5.1%  $\text{CO}_2$ , the  $\alpha_{\text{CO}_2/\text{N}_2}$  and  $P_{m,\text{CO}_2}$  of the IL membrane were 24.3 and  $\sim 1.0 \times 10^{-8} \text{ mol/m}^2 \cdot \text{s} \cdot \text{Pa}$ , respectively, at 26  $^{\circ}\text{C}$ ;

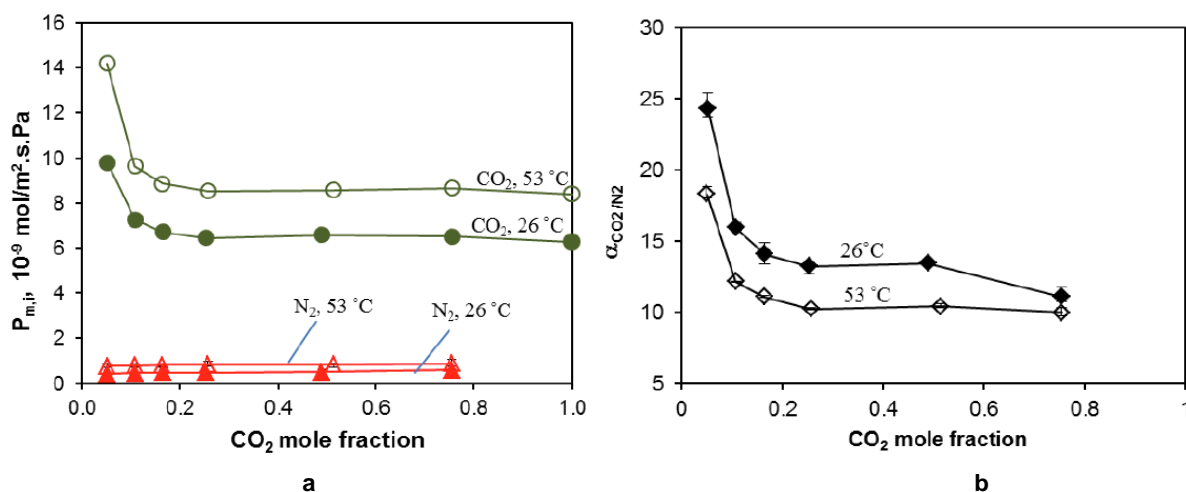


**Figure 6:** Results of CO<sub>2</sub> separation by the SIL-IL20 membrane as a function of CO<sub>2</sub> mole fraction in the feed: (a) permeance ( $P_{m,i}$ ) and (b) separation factor ( $\alpha_{\text{CO}_2/\text{N}_2}$ ).

and were 18.3 and  $1.4 \times 10^{-8} \text{ mol/m}^2 \cdot \text{s} \cdot \text{Pa}$ , respectively, at 53 °C. At both temperatures, the  $P_{m,\text{CO}_2}$  and  $\alpha_{\text{CO}_2/\text{N}_2}$  decreased significantly when  $x_{\text{CO}_2}$  increased from 5.1% to ~ 20% but tended to level off when  $x_{\text{CO}_2}$  further increased above 20%. The  $x_{\text{CO}_2}$ -dependence (or CO<sub>2</sub> partial pressure-dependence) of  $P_{m,\text{CO}_2}$  shown in Figure 6 generally agrees with the relationship between CO<sub>2</sub> permeability and partial pressure reported in literature, which is typical for facilitated gas transport in IL membrane [18,19]. The decreases of  $P_{m,\text{CO}_2}$  and  $\alpha_{\text{CO}_2/\text{N}_2}$  have been attributed to the saturation of the anionic carriers ( $\text{F}^-$ ) for CO<sub>2</sub> at high CO<sub>2</sub> partial pressures that results in smaller carrier potential gradient to reduce the CO<sub>2</sub> permeation through the IL membrane [20]; on the contrary, permeance of the physically adsorbed N<sub>2</sub> can be enhanced due to diffusivity enhancement by the reduced IL viscosity under high CO<sub>2</sub> concentration.

### 3.4. Separation of Mixtures with Impurities

The coal-firing flue gases contain typical impurities such as water vapor and trace SO<sub>x</sub> etc., which may be absorbed by the IL and adsorbed by the nanoporous silicalite to change gas transport properties in the silicalite-supported IL membrane. CO<sub>2</sub> separation was performed on the SIL-IL20 membrane at 50 °C and atmospheric pressure for CO<sub>2</sub>/N<sub>2</sub> binary mixtures with different  $x_{\text{CO}_2}$  of 0.1, 0.3, 0.5, and 0.7 (on dry gas basis), respectively, and partial pressures of water vapor of 5.6 and 9.0 kPa, respectively. The results are shown in Figure 7. The presence of water in the feed improved the CO<sub>2</sub> permeance and CO<sub>2</sub>/N<sub>2</sub> selectivity for feed streams of low CO<sub>2</sub> concentrations. These results are in agreement with findings in the literature where the increase of CO<sub>2</sub> permeance in the water-containing IL membranes was attributed to the consequential reduction of viscosity that increased the

CO<sub>2</sub> diffusivity [21] and facilitated the IL surface renewal to enhance the rate of CO<sub>2</sub> dissolving from gas into IL phase. Zhao *et al.* reported that the existence of water caused slight decrease in CO<sub>2</sub> solubility but the increase of diffusivity had an overpowering effect leading to an increase of permeability; on the other hand, although the diffusivity of N<sub>2</sub> also increased in the water-containing [bmim][BF<sub>4</sub>], N<sub>2</sub> permeance was essentially unchanged, maybe due to its very low solubility [21]. These led to an increase in  $\alpha_{\text{CO}_2/\text{N}_2}$ . The silicalite surface is known to be hydrophobic and thus the existence of water vapor has rather minor influence on the transport of the adsorbing CO<sub>2</sub> and non-adsorbing N<sub>2</sub> through the zeolitic pores. For feed gases of high CO<sub>2</sub> concentration, the effect of water content on CO<sub>2</sub> separation was much less pronounced possibly because of increased formation of bicarbonate [ $\text{HCO}_3^-$ ] ions, which have smaller diffusivity in the IL and are more difficult to be released from the IL as compared to the molecular CO<sub>2</sub> that counters the effect of water on CO<sub>2</sub> diffusivity enhancement. On the other hand, the existence of water had much smaller impact on the permeance of the inert N<sub>2</sub> in the entire range of concentration. Therefore, when water was added, the  $\alpha_{\text{CO}_2/\text{N}_2}$  increased significantly for mixtures of low CO<sub>2</sub> concentrations but remained virtually unchanged for mixtures of high CO<sub>2</sub> concentrations.

A multicomponent mixture containing 500 ppmv SO<sub>2</sub> and 20% CO<sub>2</sub> in balance air was fed to test the effect of trace SO<sub>2</sub> on the CO<sub>2</sub> separation by the IL membrane. The separation results are presented in Figure 8. The presence of 500 ppmv SO<sub>2</sub> in the feed stream slightly lowered the CO<sub>2</sub> and N<sub>2</sub> permeance but did not cause appreciable changes to the CO<sub>2</sub>/air separation factor. Similar observations on the effect of SO<sub>2</sub> on CO<sub>2</sub> separation in IL were reported in the literature where the small decrease of  $P_{m,\text{CO}_2}$  was

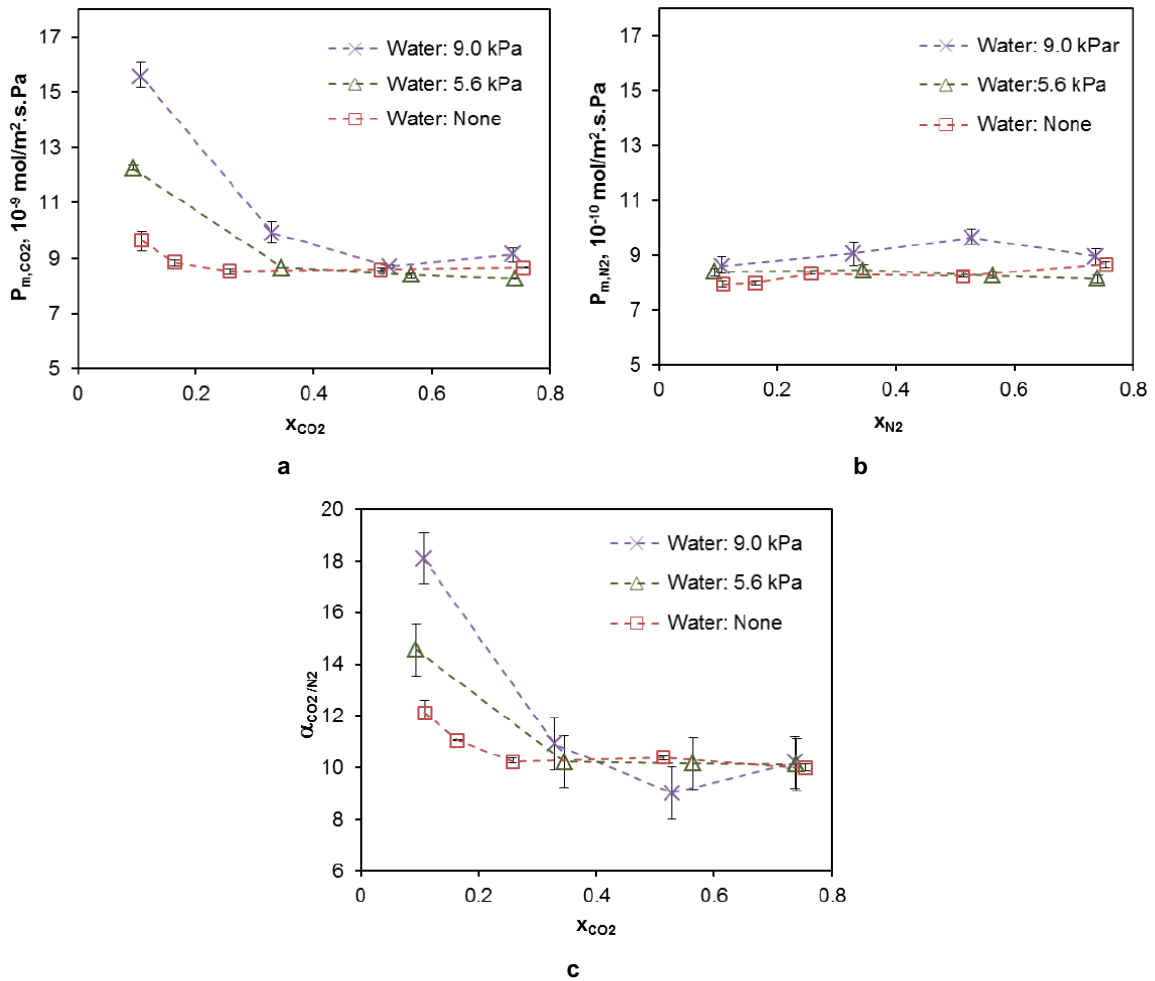


**Figure 7:** Separation of CO<sub>2</sub>/N<sub>2</sub> mixtures at 50 °C with different water contents in the feed: (a)  $P_{m,CO_2}$ , (b)  $P_{m,N_2}$ , and (c)  $\alpha_{CO_2/N_2}$ .

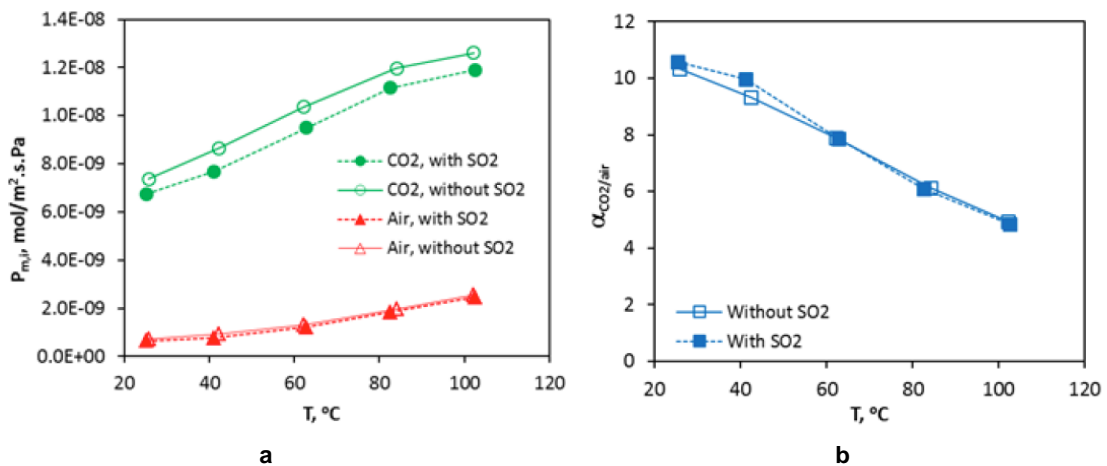


**Figure 8:** CO<sub>2</sub> separation for mixtures containing 20% CO<sub>2</sub> and 80% air with and without 500 ppmv SO<sub>2</sub>: (a) gas permeance and (b) CO<sub>2</sub>/air separation factor.

attributed to the hindrance for CO<sub>2</sub> diffusion in the IL by the dissolved SO<sub>2</sub> as well as possible increase in resistance for CO<sub>2</sub> dissolution at the gas/IL interface where ionic carriers for CO<sub>2</sub> are partially consumed by the SO<sub>2</sub> [22].

Figure 9 shows the IR spectra for the [bmim][BF<sub>4</sub>] IL after absorption and desorption of different gases. As expected, the inert N<sub>2</sub> is physically dissolved into the [bmim][BF<sub>4</sub>] that does not cause any change in the IR spectrum of the IL. After being exposed to CO<sub>2</sub>, the IR

spectrum showed CO<sub>2</sub> peaks at wavenumber of 2342 cm<sup>-1</sup> but no new peaks besides those of the IL were observed, meaning that CO<sub>2</sub> is physically absorbed as well. After contacting with saturate water vapor (~3%) at 25 °C, the characteristic IR absorption peaks for water appeared at wavenumber of 1634 and 3626 cm<sup>-1</sup>. Although SO<sub>2</sub> is reported to dissolve in [bmim][BF<sub>4</sub>] by physical absorption [23], no SO<sub>2</sub> peaks were appreciable after the IL sample was exposed to the air stream containing 500 ppmv SO<sub>2</sub>, which was perhaps a result of the extremely low SO<sub>2</sub> concentration (undetectable by the GC in our lab). It should be noted that the solubility of SO<sub>2</sub> in the [bmim][BF<sub>4</sub>] is only 0.1wt% even when equilibrated in 1 bar of pure SO<sub>2</sub> atmosphere at 40 °C [24]. In all cases, no new IR absorption peaks appeared other than the characteristic peaks of the pure [bmim][BF<sub>4</sub>] and individual gases. This confirms that gases involved in this work had no strong chemical interactions with the IL. The characteristic peaks of CO<sub>2</sub> and water completely disappeared after the degassing process that explains the good reversibility of the SIL-IL20 membrane in permeation of various gases [25].

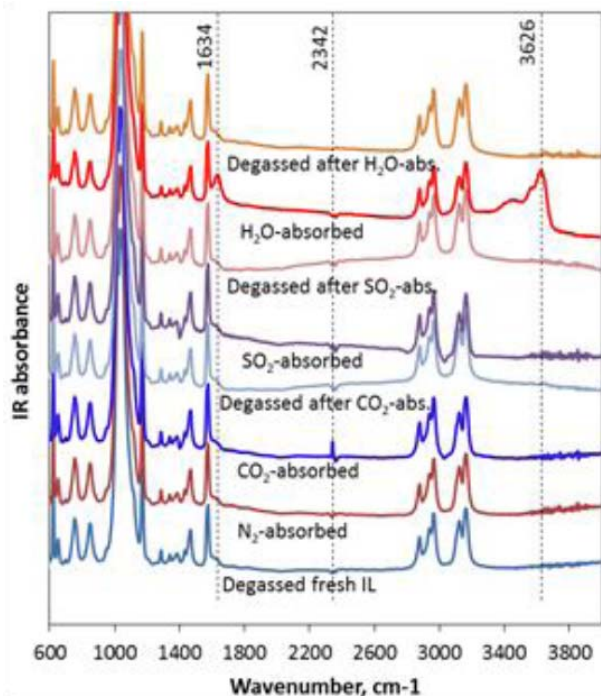


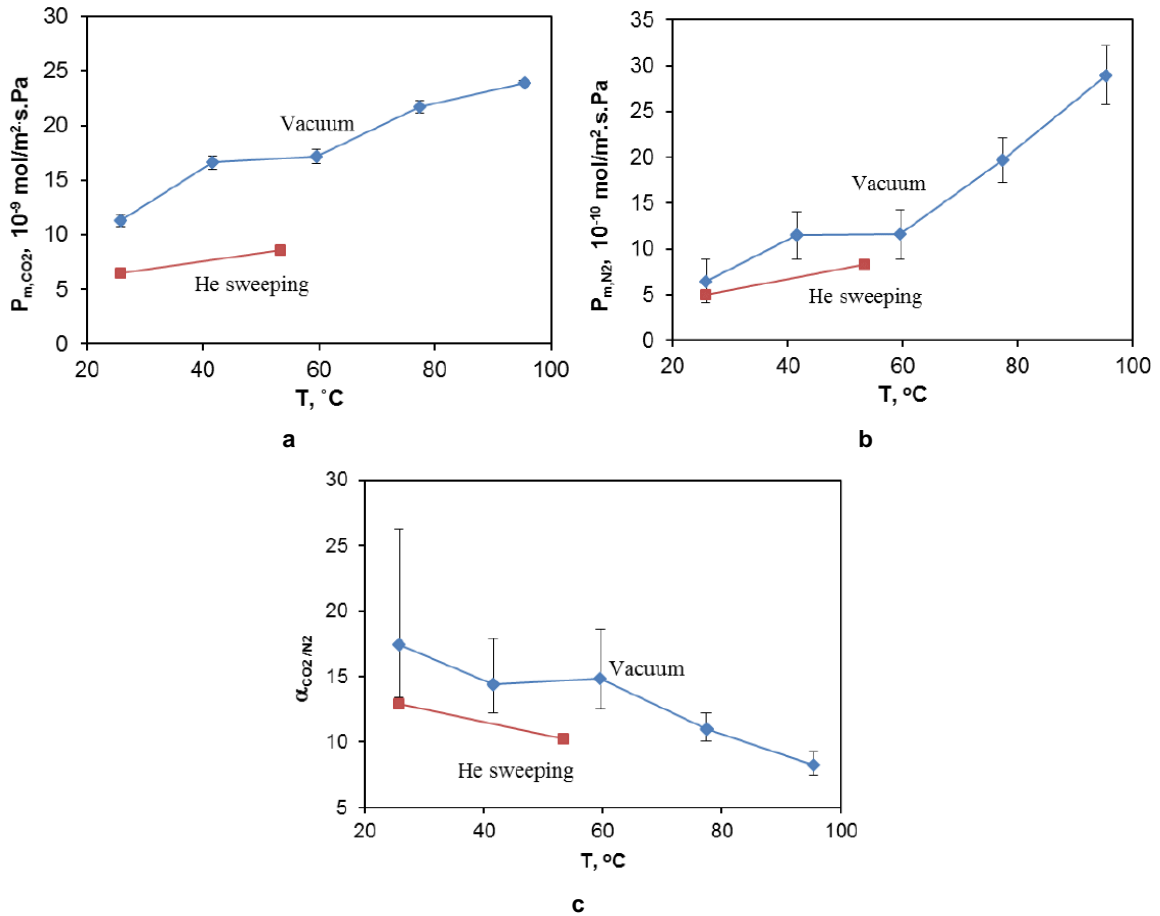
**Figure 9:** IR spectra of IL samples after absorption and desorption of different gases.

### 3.5. Separation under Different Pressure Conditions

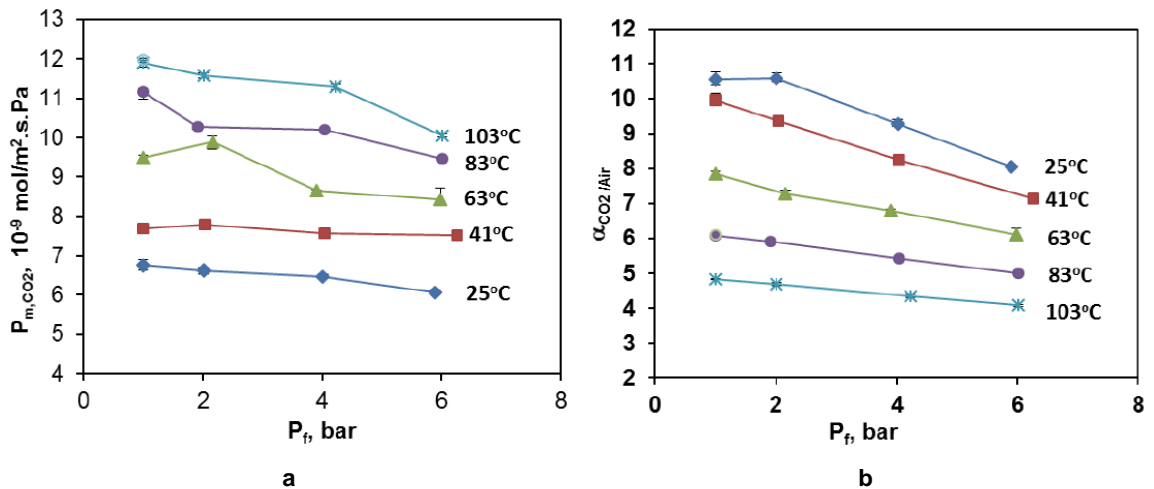
The results of CO<sub>2</sub> separation from the equimolar mixture of CO<sub>2</sub>/N<sub>2</sub> by the SIL-IL20 membrane under different downstream conditions are presented in

Figure 10. It was found that the permeance of both CO<sub>2</sub> and N<sub>2</sub> were higher when downstream was vacuumed than were they under helium sweeping flow at downstream. The increase of permeance was more significant for CO<sub>2</sub> than N<sub>2</sub> that resulted in an enhanced separation factor. This may be explained taking into account the different gas transport mechanisms through the macroporous substrate (facing downstream) under the two operation conditions. When being swept by a helium flow, the permeating gases diffuse through the essentially stagnant gas in the substrate pores driven by partial pressure gradients; while under vacuum pressure, the permeating gases transport through the substrate pores by both molecular diffusion under partial pressure gradients and viscous flow driven by total pressure difference between the inside and outside of the substrate. Thus removal of the permeating gases is more efficient under downstream vacuum pressure. This results in smaller partial pressures of permeating gas at the downstream IL/gas interface, and hence greater driving force across the IL film, which facilitates the gas transport. Moreover, the gas permeance may be also enhanced at downstream vacuum pressure due to the elimination of counter diffusion of the sweeping helium in the IL membrane.

The SIL-IL20 membrane was further tested for separation of the multicomponent mixture containing 20% CO<sub>2</sub>, 500 ppmv SO<sub>2</sub> and balance air in a temperature range of 25 – 103 °C while the feed pressure was varied from 1 bar to ~ 6 bar but using a downstream helium sweep flow at 1 bar. The results are shown in Figure 11. The highest feed pressure tested in this work was limited by the sealing O-rings, which weakens at >100°C under high pressures, but not due to damage or eruption of the liquid membrane. The supported IL membrane remained perfectly stable under the 5-bar total differential pressure ( $\Delta P$ ) even at 103 °C. The excellent resistance to  $\Delta P$  is attributed to the strong capillary action in the small pores of the colloidal silicalite layer. The colloidal silicalite membrane-supported [bmim][BF<sub>4</sub>] IL membrane was operated for nearly one year in the present work without reloading IL. The membrane sustained a differential pressure of 5 bars at 103 °C for several days with no indication of IL film rupturing. Figure 11 shows that  $P_{m,CO_2}$  tends to decrease slightly with increasing the feed pressure that may be explained similarly to the discussion for the dependence of  $P_{m,CO_2}$  on the CO<sub>2</sub> partial pressure in section 3.3, namely the diminishing free carriers for CO<sub>2</sub> at high CO<sub>2</sub> partial pressure. Also, it has been reported that the solubility



**Figure 10:** Separation of the CO<sub>2</sub>/N<sub>2</sub> equimolar mixture as a function of temperature under different downstream conditions: (a) CO<sub>2</sub> permeance, (b) N<sub>2</sub> permeance, (c) CO<sub>2</sub>/N<sub>2</sub> separation factor.



**Figure 11:** Results of CO<sub>2</sub> separation from the multicomponent mixture as a function of feed pressure at different temperatures.

and diffusivity of CO<sub>2</sub> in [bmim][BF<sub>4</sub>] decrease slightly with increasing CO<sub>2</sub> pressure [16]; for example, the CO<sub>2</sub> permeability ( $P_{b,CO_2}$ ) in the IL was found to decrease from  $7.16 \times 10^{-14}$  to  $6.78 \times 10^{-14}$  mol/m<sup>2</sup>·s·Pa when CO<sub>2</sub> pressure increase from 0.1 to 0.7 MPa at 25 °C.

#### 4. CONCLUSIONS

A colloidal silicalite thin layer with an average inter-particle pore size of 25 nm was coated on an alumina disc with an average pore size of ~85 nm for supporting the [bmim][BF<sub>4</sub>] IL membrane. The colloidal

silicalite layer greatly improved the formation of pinhole-free IL membrane with reduced IL load as compared to the bare alumina disc. The supported IL membrane was experimentally investigated for CO<sub>2</sub> separation under various conditions relevant to CO<sub>2</sub>-capture from coal-firing flues gases. The silicalite supported IL membrane exhibited excellent thermal and chemical stabilities and great tolerance to differential pressure that are practically desirable. However, the amount of IL needed to achieve a pinhole-free IL membrane on the silicalite-coated substrate was much greater than what was expected for filling the entire colloidal silicalite layer alone. Thus, the potential benefit of the CO<sub>2</sub>-permselective silicalite support for enhancing CO<sub>2</sub>-permeance was not realized because of the large thickness of the IL film penetrated into the alumina base substrate, which had an unfavorable PSD causing IL penetration. Research is being planned in our lab to develop macroporous ceramic supports with optimized PSD so that the IL film can be retained in the micron-thin silicalite layer without penetrating into the base substrate.

## ACKNOWLEDGEMENT

This research was supported by the Development Service Agency of Ohio through the Ohio Coal Research and Development program (Grant # OOE-CDO-D-13-28) and the National Science Foundation (CBET1263860).

## REFERENCES

- [1] Figueroa JD, Fout T, Plasynski S, McIlvried H, Srivastava RD. Advances in CO<sub>2</sub> capture technology-The U.S. Department of Energy's Carbon Sequestration Program. *J Intl Greenhouse Gas Control* 2008; 2: 9-20. [http://dx.doi.org/10.1016/S1750-5836\(07\)00094-1](http://dx.doi.org/10.1016/S1750-5836(07)00094-1)
- [2] Zhai H, Rubin ES. Comparative Performance and Cost Assessments of Coal and Natural Gas fired Power Plants under a CO<sub>2</sub> Emission Performance Standard Regulation. *Energy Fuels* 2013; 27: 4290-4301. <http://dx.doi.org/10.1021/ef302018v>
- [3] Zhang X, He X, Gundersen T. Post-combustion Carbon Capture with a Gas Separation Membrane: Parametric Study, Capture Cost, and Exergy Analysis. *Energy Fuels* 2013; 27: 4137-4149. <http://dx.doi.org/10.1021/ef3021798>
- [4] Privalova EI, Mañé ki-Arvela P, Murzin DY, Mikkola JP. Capturing CO<sub>2</sub>: conventional versus ionic-liquid based technologies. *Russ Chem Rev* 2012; 81: 435-457. <http://dx.doi.org/10.1070/RC2012v081n05ABEH004288>
- [5] Anderson JL, Dixon JK, Maginn EJ, Brennecke JF. Measurement of SO<sub>2</sub> solubility in ionic liquids. *J Phys Chem B* 2006; 110: 15059-15062. <http://dx.doi.org/10.1021/jp063547u>
- [6] Ramdin M, de Loos TW, Vlught TJH. State-of-the-Art of CO<sub>2</sub> Capture with Ionic Liquids. *Ind. Eng Chem Res* 2012; 51: 8149-8177. <http://dx.doi.org/10.1021/ie3003705>
- [7] Iarikov DD, Hacarlioglu P, Oyama ST. Supported room temperature ionic liquid membranes for CO<sub>2</sub>/CH<sub>4</sub> separation. *Chem Eng J* 2011; 166: 401-406. <http://dx.doi.org/10.1016/j.cej.2010.10.060>
- [8] Kim DH, Baek IH, Hong SU, Lee HK. Study on immobilized liquid membrane using ionic liquid and PVDF hollow fiber as a support for CO<sub>2</sub>/N<sub>2</sub> separation. *J Membr Sci* 2011; 372: 346-354. <http://dx.doi.org/10.1016/j.memsci.2011.02.025>
- [9] Wickramanayake S, Hopkinson D, Myers C, Sui L, Luebke D. Investigation of transport and mechanical properties of hollow fiber membranes containing ionic liquids for pre-combustion carbon dioxide capture. *J Membr Sci* 2013; 439: 58-67. <http://dx.doi.org/10.1016/j.memsci.2013.03.039>
- [10] Fredlake CP, Crosthwaite JM, Hert DG, Aki SNVK, Brennecke JF. Thermophysical Properties of Imidazolium-Based Ionic Liquids. *J Chem Eng Data* 2004; 49: 954-964. <http://dx.doi.org/10.1021/je034261a>
- [11] Tang Z, Kim SJ, Gu X, Dong J. Microwave synthesis of MFI-type zeolite membranes by seeded secondary growth without the use of organic structure directing agents. *Micropor Mesopor Mater* 2009; 118: 224-231. <http://dx.doi.org/10.1016/j.micromeso.2008.08.029>
- [12] Vroon ZAEP. Synthesis and transport properties of thin ceramic supported zeolite (MFI) membranes, Ph.D. Dissertation, University of Twente, The Netherlands 1995.
- [13] Kim SJ, Xu Z, Reddy GK, Smirniotis P, Dong J. Effect of Pressure on High-Temperature Water Gas Shift Reaction in Microporous Zeolite Membrane Reactor. *Ind Eng Chem Res* 2012; 51: 1364-1375. <http://dx.doi.org/10.1021/ie201452y>
- [14] Gong YN, Wang HT, Chen YF, Hu XH, Ibrahim AR, Tanyi AR, Hong YZ, Su YZ, Li J. A High-Pressure Quartz Spring Method for Measuring Solubility and Diffusivity of CO<sub>2</sub> in Ionic Liquids. *Ind Eng Chem Res* 2013; 52: 3926-3932. <http://dx.doi.org/10.1021/ie400267h>
- [15] Gu X, Tang Z, Dong J. On-stream modification of MFI zeolite membranes for enhancing hydrogen separation at high temperature. *Micropor Mesopor Mater* 2008; 111: 441-448. <http://dx.doi.org/10.1016/j.micromeso.2007.08.039>
- [16] Shiflett MB, Yokozeki A. Solubilities and diffusivities of carbon dioxide in ionic liquids: bmim PF<sub>6</sub> and bmim BF<sub>4</sub>. *Ind Eng Chem Res* 2005; 44: 4453-4464. <http://dx.doi.org/10.1021/ie058003d>
- [17] Hazelbaker ED, Guillet-Nicolas R, Thommes M, Kleitz F, Vasenkov S. Influence of confinement in mesoporous silica on diffusion of a mixture of carbon dioxide and an imidazolium-based ionic liquid by high field diffusion NMR. *Micropor Mesopor Mater* 2015; 206: 177-183. <http://dx.doi.org/10.1016/j.micromeso.2014.12.005>
- [18] Jindaratamee P, Ito A, Komuro S, Shimoyama Y. Separation of CO<sub>2</sub> from the CO<sub>2</sub>/N<sub>2</sub> mixed gas through ionic liquid membranes at the high feed concentration. *J Membr Sci* 2012; 423: 27-32. <http://dx.doi.org/10.1016/j.memsci.2012.07.012>
- [19] Jue ML, Lively, RP. Targeted gas separations through polymer membrane functionalization. *React Funct Polym* 2015; 88-110. <http://dx.doi.org/10.1016/j.reactfunctpolym.2014.09.002>
- [20] Hasib-ur-Rahman M, Siaj M, Larachi F. Ionic liquids for CO<sub>2</sub> capture-Development and progress. *Chem Eng Process* 2010; 49: 313-322. <http://dx.doi.org/10.1016/j.cep.2010.03.008>
- [21] Zhao W, He GH, Zhang LL, Ju J, Dou H, Nie F, Li CN, Liu HJ. Effect of water in ionic liquid on the separation performance of supported ionic liquid membrane for CO<sub>2</sub>/N<sub>2</sub>. *J Membr Sci* 2010; 350: 279-285. <http://dx.doi.org/10.1016/j.memsci.2010.01.002>

- [22] Okabe K, Matsumiya N, Mano H. Stability of gel-supported facilitated transport membrane for carbon dioxide separation from model flue gas. *Sep Purif Technol* 2007; 57: 242-249. <http://dx.doi.org/10.1016/j.seppur.2007.04.007>
- [23] Huang J, Riisager A, Wasserscheid P, Fehrmann R. Reversible physical absorption of SO<sub>2</sub> by ionic liquids. *Chem Commun* 2006; 4027-4029. <http://dx.doi.org/10.1039/B609714F>
- [24] Wu W, Han B, Gao H, Liu Z, Jiang T, Huang J. Desulfurization of Flue Gas: SO<sub>2</sub> Absorption by an Ionic Liquid. *Angew Chem Int Ed* 2004; 43: 2415-2417. <http://dx.doi.org/10.1002/anie.200353437>
- [25] Andanson JM, Jutz F, Baiker A. Purification of ionic liquids by supercritical CO<sub>2</sub> monitored by infrared Spectroscopy. *J Supercrit Fluids* 2010; 55: 395-400. <http://dx.doi.org/10.1016/j.supflu.2010.08.012>

---

Received on 08-02-2016

Accepted on 02-03-2016

Published on 06-04-2016

DOI: <http://dx.doi.org/10.6000/1929-6037.2016.05.01.3>

© 2016 Cao *et al.*; Licensee Lifescience Global.

This is an open access article licensed under the terms of the Creative Commons Attribution Non-Commercial License (<http://creativecommons.org/licenses/by-nc/3.0/>) which permits unrestricted, non-commercial use, distribution and reproduction in any medium, provided the work is properly cited.